


## Article

# Hydrothermal Synthesis of Cellulose Nanocrystal-Grafted-Acrylic Acid Aerogels with Superabsorbent Properties

Xuehua Liu <sup>1</sup>, Rue Yang <sup>2</sup>, Mingcong Xu <sup>1</sup>, Chunhui Ma <sup>1</sup>, Wei Li <sup>1,2,3,\*</sup> , Yu Yin <sup>1</sup>, Qiongtao Huang <sup>2</sup>, Yiqiang Wu <sup>3</sup>, Jian Li <sup>1</sup> and Shouxin Liu <sup>1,\*</sup>

<sup>1</sup> Key Laboratory of Bio-Based Material Science and Technology of Ministry of Education, Northeast Forestry University, Hexing Road 26, Harbin 150040, China; aliuxuehua@126.com (X.L.); m18846145637@163.com (M.X.); mchmchmchmch@163.com (C.M.); nefuyinyu@163.com (Y.Y.); nefulijian@163.com (J.L.)

<sup>2</sup> Post-Doctoral Research Center, Yihua Lifestyle Technology Co., Ltd., Shantou 515834, China; yangre@yihua.com (R.Y.); huangqt@yihua.com (Q.H.)

<sup>3</sup> School of Materials Science and Engineering, Central South University of Forestry and Technology, Changsha 410004, Hunan, China; wuyq0506@126.com

\* Correspondence: liwei19820927@126.com (W.L.); liushouxin@126.com (S.L.); Tel./Fax: +86-451-82191204 (W.L.); +86-451-82191502 (S.L.)

Received: 12 September 2018; Accepted: 17 October 2018; Published: 19 October 2018



**Abstract:** In this work, we applied a fast and simple method to synthesize cellulose nanocrystal (CNC) aerogels, via a hydrothermal strategy followed by freeze drying. The characteristics and morphology of the obtained CNC-g-AA aerogels were affected by the hydrothermal treatment time, volume of added AA (acrylic acid), and the mass fraction of the CNCs. The formation mechanism of the aerogels involved free radical graft copolymerization of AA and CNCs with the cross-linker *N,N'*-methylene bis(acrylamide) (MBA) during the hydrothermal process. The swelling ratio of the CNC-g-AA aerogels was as high as 495:1, which is considerably greater than that of other polysaccharide-g-AA aerogels systems. Moreover, the CNC-g-AA aerogels exhibited an excellent methyl blue (MB) adsorption capacity and the ability to undergo rapid desorption/regeneration. The maximum adsorption capacity of the CNC-g-AA aerogels for MB was greater than 400 mg/g. Excellent regeneration performance further indicates the promise of our CNC-g-AA aerogels as an adsorbent for applications in environmental remediation.

**Keywords:** cellulose nanocrystals; hydrothermal; aerogels; superabsorbent

## 1. Introduction

Developments in industry and commerce have raised the problem of dye contamination, which is characterized by a high organic matter content, resistance to biodegradability, and complex biological toxicity [1]. Dye contamination raises serious environmental concern with potential dangers to food safety and aquatic life [2]. Various groups have tried to develop more efficient methods of removing dye pollutants. Dye pollution removal is conventionally achieved by photochemical degradation, membrane filtration, flocculation, biological oxidation, and chemical precipitation [3,4]. However, these technologies are complex and expensive; hence, the design and development of alternative low-cost adsorbents has been the focus of many studies.

Cellulose nanocrystals (CNCs) are a renewable material with properties including good biodegradability, mechanical strength [5], flexibility [6], easily modified, and biocompatibility [7,8]. The high strength, dimensional anisotropy, and natural sourcing of CNCs, have attracted considerable

research interest for their use as functional and renewable reinforcing agents for polymer composites [9,10]. The rigid and flexible mechanical properties of CNCs show great potential for various applications and have motivated research on preparing CNC aerogels for different fields [11–13]. The fabrication of CNC-based aerogels can avoid issues related to cellulose gel shrinkage, capillary tension, and rupturing in drying processes owing to capillary pressure [14]. Functionalized CNC aerogels can exhibit multiple responses according to changes in external conditions, such as temperature, pH, and pressure [15,16]. Thus, CNC aerogels can be used in biological applications and as strained materials, adsorbent materials, hydrophobic materials, and conductive materials. There are also ideal materials for applications in environmental modification [17–19].

Highly porous CNC-based aerogels with many hydroxyl groups are widely regarded as superabsorbent materials [20]. The unique properties of these materials include high strength, high surface area, and tunable surface chemistry, which enable interactions with other polymers. In particular, functional polymeric materials, containing a strong hydrophilic group introduced by graft copolymerization reactions, are widely used in polysaccharide reaction systems because of their high efficiency and compatibility. CNC-based aerogels can be prepared by a free chain graft polymerization with poly-methacrylic acid, which is modified by functionalizing the carboxylic group [21]. CNC-based aerogels can also be prepared by free radical polymerization of poly(*N*-isopropylacrylamide) (PNIPAM) and grafted by copolymerization of poly (acrylic acid) (PAA), to achieve functionalization by cooperative hydrogen bonding interactions between PNIPAM or PAA and the CNCs [16,22]. Moreover, CNCs, which are graft-copolymerized with AA (acrylic acid) give hydrogels with a swelling ratio far greater than that of other polysaccharide systems combined with AA hydrogels, at the same initial reactant ratio [23,24].

Recently, hydrothermal procedures to produce hydrogels from cellulosic biomass have received attention owing to their inherent advantages in terms of liquid chemical reactions and their simplicity [25]. Compared with reactions at ambient temperature and pressure, the straight forward hydrothermal method developed here requires less reagents to promote the reaction to completion. Our group has prepared fluorescent CNC/carbon dot hydrogels by a one-step hydrothermal method [26]. The shape and chemical structure of the products can also be controlled by the hydrothermal method. Hydrothermal methods are considered to be highly effective for fabricating CNC-based hydrogels [27,28]. These results encouraged us to use a hydrothermal strategy to promote a graft-copolymerized reaction to synthesize a CNC-based aerogel superabsorbent.

In this study, we proposed a simple method to fabricate CNC-g-AA aerogels via a hydrothermal treatment followed by freeze drying. We examined the swelling performance of the obtained aerogels for the water absorption and the adsorption properties of the CNC-g-AA aerogels for methylene blue (MB).

## 2. Materials and Methods

### 2.1. Materials

The CNCs were prepared from commercial bleached kraft softwood pulp (85% International Standardization Organization brightness) as the raw material, which was provided by a paper-making factory in Heilongjiang, China. Analytical-grade sulfuric acid was purchased from Tianjin Kermel Chemical Reagent Co., Ltd. (Tianjin, China). Tetramethylethylenediamine (TMEDA), *N,N'*-methylene bis(acrylamide) (MBA), and ammonium persulfate (APS) were purchased from Aladdin Reagent Corp China (Chengdu, Sichuan Province, China). The AA and MB were purchased from Tianjin Fuchen Chemical Reagent Factory (Tianjin, China). All chemical reagents were of analytical grade.

### 2.2. Preparation of CNC-g-AA Hydro/Aerogels

An aqueous CNCs suspension was prepared by a sulfuric acid hydrolysis method, as previously reported [29,30]. Bleached kraft softwood was first milled and then passed through a 0.5-mm screen to

ensure a uniform particle size. Then, the milled pulp was hydrolyzed in sulfuric acid (64 wt %; 8.75 mL of sulfuric acid solution per gram of pulp) at 45 °C for 30 min with vigorous stirring. The cellulose suspension was then diluted, centrifuged, washed, and dialyzed against distilled water until the exterior water became neutral before further use.

The CNC-g-AA hydrogels were prepared by a free radical graft copolymerization of CNCs and AA in the presence of a cross-linker (MBA) and a redox initiator system (APS/TMEDA). A 10 mL portion of the prepared CNC solution (1.5 wt %) was placed in a 100 mL three-necked flask, which was then placed in a 25 °C water bath and stirred with a magnetic stirrer. A 0.050 g portion of APS and 0.050 mL of TMEDA, as an initiator, were added to the solution and the mixture was stirred for 10 min to generate radicals. Thereafter, a cross-linker, MBA (0.080 g) and a certain volume of AA were added, followed by continuous stirring for 2 h. The reaction solution was then placed in a Teflon-lined stainless steel autoclave (100 mL) and heated to the desired temperature. The hydrothermal reaction was performed for a specific time. The obtained gels were washed in distilled water to remove unreacted substances.

Thereafter, the as-prepared hydrogels were frozen in liquid nitrogen. After complete freezing, the frozen samples were subjected to freeze-drying (Scientz-10N, Ningbo, Zhejiang Province, China) to obtain pristine CNCs-g-AA aerogels. The resulting CNC-g-AA hydro/aerogels are referred to as CNC-g-AA-r-m-n, where r denotes the AA content, m denotes the hydrothermal temperature, and n denotes the hydrothermal time. Furthermore, we prepared pure hydro/aerogels, where the CNCs solution was replaced with distilled water under conditions of 2.0 mL AA, a hydrothermal temperature of 120 °C, and a treatment time of 8 h (D-g-AA-2-120-8 hydro/aerogels). Herein, the swelling of CNC-g-AA-2-120-8 gel performance in distilled water is shown in Figure 1.

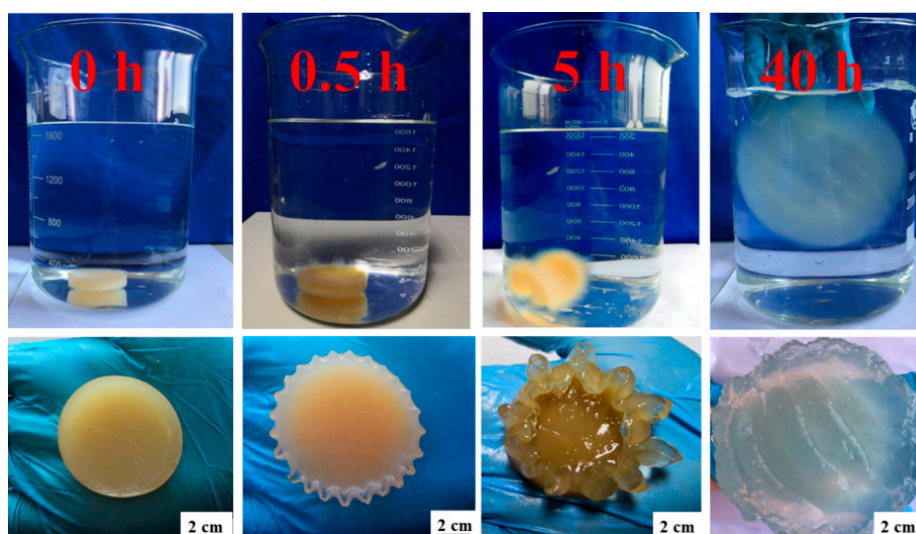


**Figure 1.** Photographs showing swelling and size-change of CNC-g-AA-2-120-8 gel in distilled water over time.

### 2.3. Characterization of CNC-g-AA Aerogels

FT-IR spectra of CNC-g-AA aerogels were measured on a Fourier transform infrared spectrometer (iS10, Nicolet, Thermo Scientific, Waltham, MA, USA) over the range of 400–4000  $\text{cm}^{-1}$  in transmission mode. For morphological studies, we examined the CNC-g-AA aerogels with a scanning electron microscope (SEM, QUANTA200, FEI, Hillsboro, OR, USA). Specimens were coated with gold before SEM observations. The  $^{13}\text{C}$  CP/MAS NMR analysis of the samples was performed at room temperature with a Bruker DRX-400 spectrometer. Spectra were acquired with a 4-mm MAS probe using a combination of CP, MAS, and high-power proton decoupling methods. A total of 800 scans were accumulated for each sample.

#### 2.4. Swelling Characterization of CNC-g-AA Aerogels in Distilled Water

The equilibrium swelling ratios of the CNC-g-AA aerogels were measured in distilled water at room temperature. A portion of the CNC-g-AA aerogels ( $W_1$ ) was then prepared and immersed in an excess of distilled water to achieve a state of equilibrium swelling. The weight gain of the equilibrium samples ( $W_2$ ) was monitored gravimetrically. Excess water on the surface of the hydrogels was removed with filter paper. Three replicates were performed for each composition. The swelling ratio was calculated by the following Equation:

$$SR = \frac{(w_2 - w_1)}{w_1} \quad (1)$$

#### 2.5. Adsorption Studies

We selected the CNC-g-AA-2-120-8 aerogel for the adsorption experiments under different experimental conditions. All experiments were performed in glass vials placed in a controlled-temperature water bath oscillator operating at 150 rpm. The MB solutions of different concentrations were prepared with distilled water. The pH of the dye solutions was adjusted with 0.01 M HCl or NaOH. After dye adsorption equilibrium was reached, we filtered the swollen gels and the residual concentration of filtered MB solution was measured with a UV-vis spectrophotometer (Evolution 600, Thermo Scientific Inc., Madison, WI, USA) and calculated from the absorption intensity at 664 nm. The amount of adsorbed MB was calculated based on the following Equation:

$$q_e = (c_0 - c_e) \frac{V}{m} \quad (2)$$

where  $q_e$  (mg/g) is the amount of the adsorbed dye at equilibrium;  $c_0$  (mg/L) and  $c_e$  (mg/L) are the initial and residual concentrations of the dye solution at equilibrium, respectively;  $V$  (L) is the volume of the dye solution; and  $m$  (g) is the mass of the adsorbent used.

We selected CNC-g-AA-2-120-8 aerogel for regeneration testing under conditions of MB solution of 20 mg/L, pH = 8.0, adsorbent mass is 0.0050 g. Here, HCl (1 mol/L) was used as the eluent. The CNC-g-AA-2-120-8 hydrogel was loaded with MB and treated with the eluent (50 mL) for 120 min at room temperature. The desorbed adsorbent was washed, freeze-dried, and prepared for the next cycle of regeneration testing.

### 3. Results and Discussion

#### 3.1. Morphology of CNC-g-AA Aerogels

The SEM images of D-g-AA aerogel and CNC-g-AA-r-m-n aerogels (Figure 2) showed three-dimensional interconnected honeycomb open-cell structures. The cell wall surfaces of D-g-AA aerogel, without added CNCs, were smooth (Figure 2a,b). For the aerogels with added CNCs, the surface of the aerogel cell walls became wrinkled. Additionally, some web-like structures formed on the cell walls, which likely improved the accessibility of water into the cell. The effects of the hydrothermal treatment time might be related to the CNCs having many active –OH groups and modified –COOH groups on their surfaces, which affected the polymerization of the composites and the formation of the three-dimensional polymer network [31,32]. For longer hydrothermal treatment times, –CO-NH– in MBA tended to combine with carboxyl groups, which contributed to the formation of a three-dimensional honeycomb network [33]. This extended dislocation structure was caused by vacancy motion at the nanoscale in the mixed liquid crystal lattice, which is conducive to the formation of a three-dimensional macroporous structure in the CNCs mixture [34,35]. This type of chemical modification can increase the hydrophilicity of CNCs and their compatibility with hydrophilic polymer matrices. Pores are regions where water can permeate, which allows interactions of external compounds with the hydrophilic groups of the graft copolymers [36].



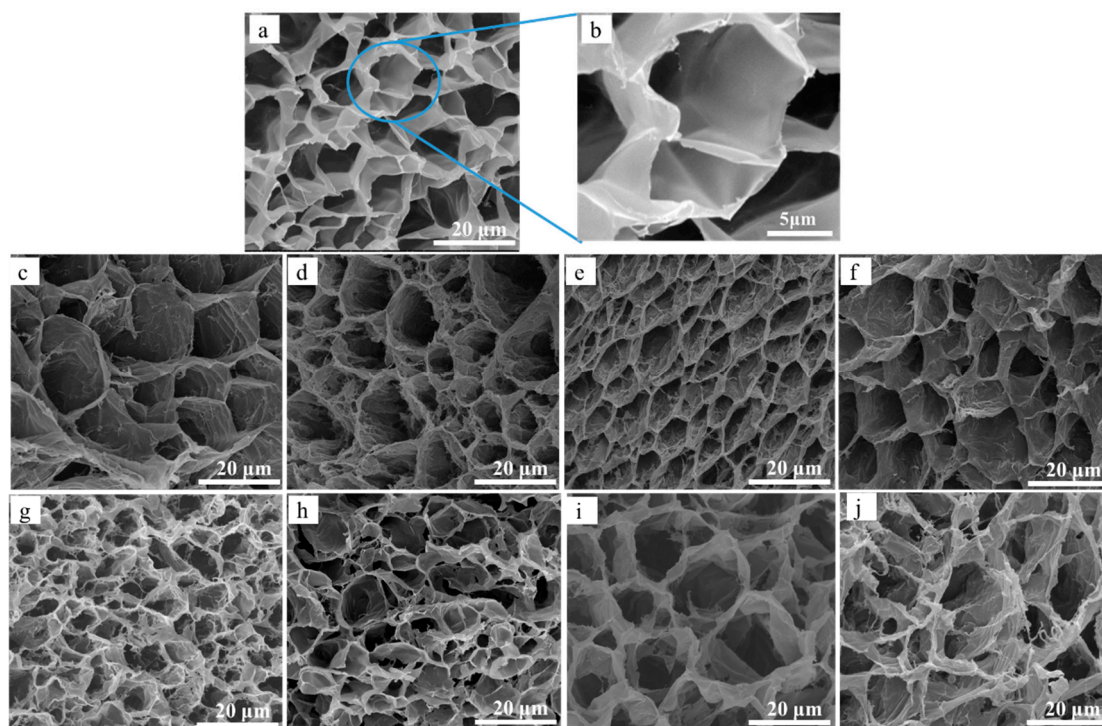


**Figure 2.** SEM images of (a,b) D-g-AA-2-120-8 aerogel; (c–f) CNC-g-AA-r-120-8 aerogels prepared with different AA contents (1, 2, 3, and 4 mL); (g–j) CNC-g-AA-2-120-n aerogels with different hydrothermal treatment times (2, 4, 8, and 12 h).

### 3.2. FT-IR and NMR Characterization of CNC-g-AA Aerogels

FT-IR spectra of pure CNCs, D-g-AA-2-120-8 aerogel, and CNC-g-AA-2-120-8 aerogel, are shown in Figure 3a. In spectrum a, peaks at 1058, 1427 and  $3337\text{ cm}^{-1}$  are associated with CNCs [37]. The peaks at 3337 and  $1026\text{ cm}^{-1}$  correspond to the O–H stretching vibration and deformation vibration peaks, indicating strong hydrogen-bonding interactions of CNCs [38]. The region of low intensity bands between 1058 and  $1427\text{ cm}^{-1}$  suggests the presence of C–O and C–H bonds [39]. In spectra b and c, we assign the peak at  $1550\text{ cm}^{-1}$  to the stretching vibration of N–H. The sharp band at  $1705\text{ cm}^{-1}$  is assigned to a symmetrical stretching vibration of  $\text{COO}^-$ , which indicated the presence of  $\text{COO}^-$  groups in the CNC-g-AA-2-120-8 aerogel network. These results confirmed that the AA monomers were successfully grafted onto the backbone of CNCs and confirmed our interpretation of the formation of the three-dimensional network structure.

To further illuminate the structure of CNC, D-g-AA and CNC-g-AA, the samples were characterized by  $^{13}\text{C}$  CP/MAS NMR spectroscopy (Figure 3b). The spectra of CNC displayed the typical signals from cellulose, which were assigned as follows: the C1 (104.7 ppm), C2/C3/C5 (71.9 and 74.9 ppm), C4 (89.1 ppm), and C6 (65.6 ppm) peaks correspond to the carbon atoms of the glucopyranose rings in the crystalline regions, whereas the C4 (84.7 ppm) peak corresponds to those in the amorphous areas [40]. For CNC-g-AA-2-120-8, the peak at 177.5 ppm is associated with carbon atoms of carboxylic acid groups, the peak at 61.9 ppm for N–CH<sub>2</sub>–CH<sub>2</sub>–O– which supports the occurrence of grafting reaction between the hydroxyl groups of CNC and MBA. So, it is apparent that the poly (acrylic acid) chains have been successfully cross-linked on CNC in the presence of the MBA cross-linker [41].

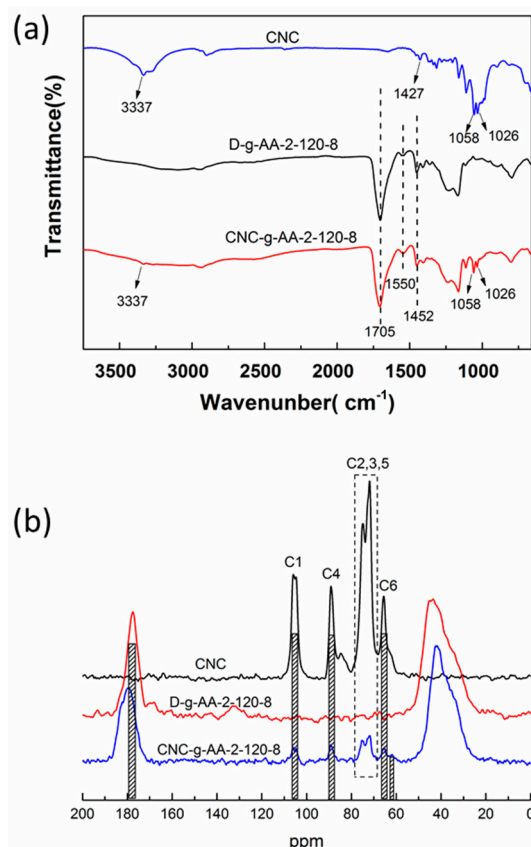


**Figure 3.** FT-IR (a) and <sup>13</sup>C NMR (b) spectra of CNC, D-g-AA-2-120-8 aerogels and CNCs-g-AA-2-120-8 aerogels.

### 3.3. Equilibrium Swelling Ratio in Distilled Water

The equilibrium swelling ratio of the CNC-g-AA-r-120-n aerogels was also related to AA content and hydrothermal reaction time (Figure 4a,b). As the amount of added AA was increased from 1.0 to 4.0 mL, the swelling ratio of the CNC-g-AA-r-120-8 aerogels increased from 174 to 495. As the hydrothermal reaction time was increased from 2 to 10 h, the swelling ratio of the resulting aerogels increased from 46 to 478. Hence, we selected the CNC-g-AA-2-120-8 aerogels for detailed analysis of their water and MB adsorption properties.

The times required for the CNC-g-AA-2-120-8 and D-g-AA-2-120-8 aerogels to reach equilibrium are shown in Figure 4c. The swelling ratio of the CNC-g-AA-aerogel was almost nine times as great as that of the D-g-AA-2-120-8 aerogel at absorption equilibrium. We attribute this difference to the incorporation of CNCs into the gel matrix, which promoted the formation of a porous and honeycomb morphology. The CNCs supported the polymer network and provided sites for the initiation of polymerization, which opened up the aerogel structure and thus contributed to the absorption capacity and swelling rate of the hydrogels [42]. In addition, the presence of CNCs in the hydrogel matrix increased the amounts of hydrophilic groups, which enabled faster and easier diffusion of aqueous solution into the hydrogel matrix [43,44].

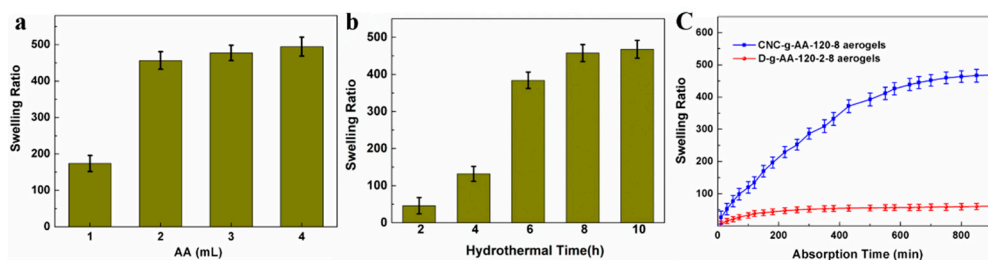


**Figure 4.** (a) Swelling ratio of CNC-g-AA-r-120-8 aerogels with different AA contents; (b) Swelling ratio of CNC-g-AA-2-120-n aerogels hydrothermally treated for different times; (c) Adsorption capacity of D-g-AA-2-120-8 aerogels and CNC-g-AA-2-120-8 aerogels compared with the adsorption time.

### 3.4. Formation Mechanism of CNC-g-AA Aerogels

A proposed mechanistic pathway for the formation of CNC-g-AA aerogels is shown in Figure 5. Sulfate anion radicals generated from APS abstracted protons from  $\text{-OH}$  groups of the CNC backbone to form alkoxy radicals, which resulted in active centers on the CNCs backbone that radically initiated polymerization. The CNCs are rich in  $\text{-OH}$  groups, which induce strong molecular interactions in the nanocomposite system [45]. After AA is added to the nanocomposites the AA becomes conjugated with the CNCs and contributes more effective binding sites. The presence of the cross-linking reagent (MBA) results in the formation of a copolymer network, which comprises a chemical cross-linked structure [46]. During the hydrothermal treatment of the CNCs with the composites, the presence of  $\text{-COO}^-$ , which is formed by deprotonation of  $\text{-COOH}$  groups, localizes the negative charge of the polymer network and enhances electrostatic repulsion, which favors expansion of the chain network. However, owing to the chemical composition of the CNC molecules, the attached  $\text{-OH}$  functional groups might induce hydrogen bond formation, which is an additional factor that improves adhesive properties [47].

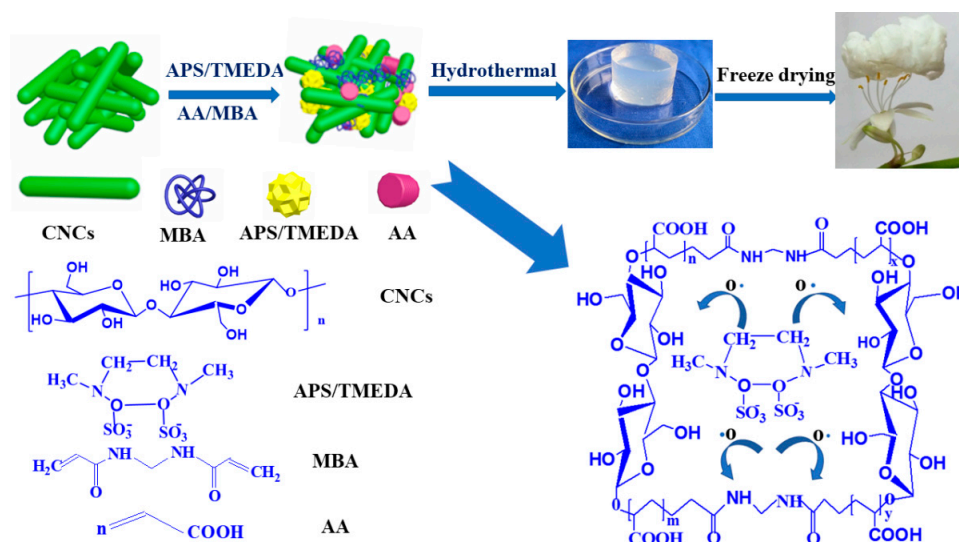


**Figure 5.** Mechanistic diagram of CNC-g-AA aerogel formation.

### 3.5. Adsorption Studies

#### 3.5.1. Studies on Dye Adsorption

The effects of the solution pH of the initially prepared MB solutions on MB dye removal (%) and the residual concentration ( $C_e$ ) of the MB after adsorption by our CNC-g-AA-2-120-8 aerogels, are shown in Figure 6a. Here, we used a 0.0050-g portion of the CNC-g-AA-2-120-8 aerogel in 50 mL of a 60 mg/L MB solution. When the solution pH was decreased from 8.0 to 3.0, the ratio of MB

removal decreased from 98.4% to 20.6% and the  $C_e$  decreased from 0.8 to 39.7 mg/L. We attribute the low adsorption ability at low pH to the CNC-g-AA-2-120-8 aerogels being immersed in an acidic environment having a more positive net charge at its surfaces, which electrostatically repelled MB.

To select a suitable amount of the adsorbent, different portions of (0.0010, 0.0020, 0.0030, 0.0040, and 0.0050 g) of CNC-g-AA-2-120-8 aerogels were added to 50 mL of 60 mg/L MB solutions, and the MB removal results are shown in Figure 6b. The adsorption capacity for the MB dyes on CNC-g-AA-2-120-8 aerogels decreased from 719.8–244.7 mg/g as the dosage increased from 0.0010 to 0.0050 g. However, the MB removal rate increased from 57.6% to 97.9% as the adsorbent dosage was increased from 0.0010 to 0.0050 g. The adsorption reached a swelling equilibrium when the adsorbent dosage was 0.0040 g. We attribute this result to the greater surface area of the adsorbent and the availability of more active adsorptive sites as the amount of the CNC-g-AA-2-120-8 aerogel was increased.

The initial MB concentration and the contact time with the CNC-g-AA-2-120-8 aerogels affected the adsorption capacity and removal efficiency. The experiments were performed at 25 °C, at pH = 8, with different initial concentrations (20–100 mg/L) and different contact times (20–450 min). The results are shown in Figure 6c. The adsorption capacity clearly increased from 96.98 to 415.13 mg/g as the initial MB concentration was increased from 20 to 100 mg/L. This result was attributed to the initial MB concentration providing the necessary driving force to surmount the resistance between the aqueous and solid phases and the increase of the initial MB concentration improved interactions between dye molecules and adsorbents, which provided heterogeneous adsorption sites [48,49].

The effects of solution temperature on MB removal by CNC-g-AA-2-120-8 aerogels are shown in Figure 6d. The MB adsorption capacity of the CNC-g-AA-2-120-8 aerogels decreased slightly with increasing temperature, from 15 to 55 °C at the same initial MB concentration. The MB adsorption capacity slightly decreased from 97.74 to 96.57 mg/g as the solution temperature was increased from 15 to 55 °C at a MB concentration of 20 mg/g. The MB adsorption capacity decreased from 474.22 to 467.31 mg/g at a MB concentration of 100 mg/g. The effects of temperature on MB adsorption might be attributed to the exothermic nature of the adsorption reaction. [50]

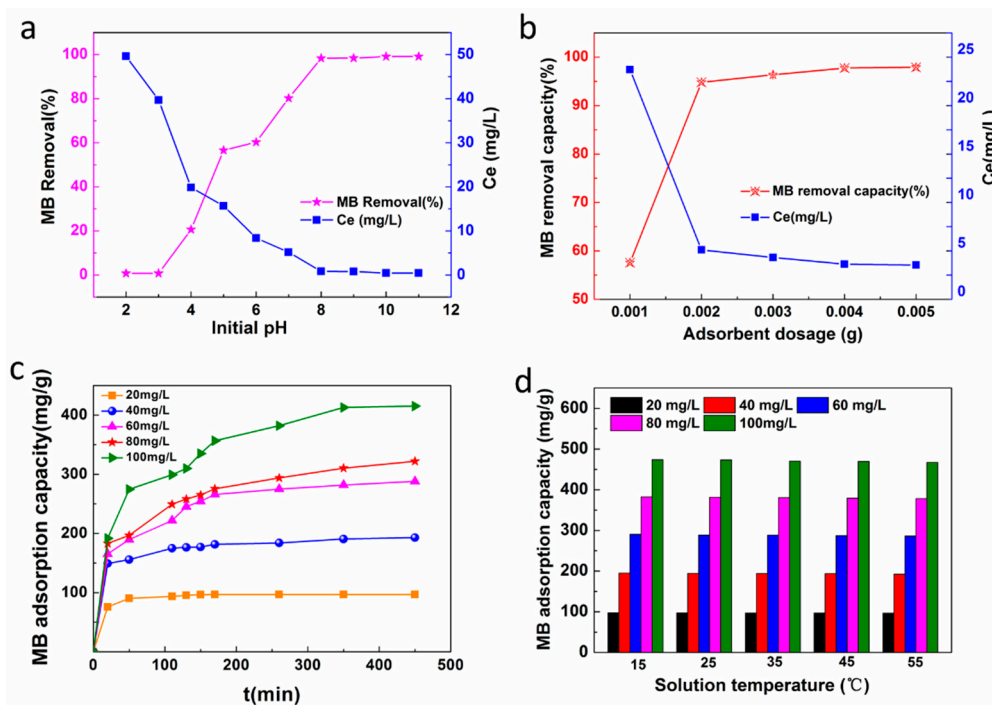


**Figure 6.** (a) Effects of solution pH on MB removal, (b) effects of adsorbent dosages on MB removal, (c) effects of contact time and initial MB solution concentration on MB adsorption, (d) effects of solution temperature on MB removal at different initial MB concentrations.



### 3.5.2. Adsorption Kinetics

The effects of the MB initial concentration and adsorption time on the CNC-g-AA-2-120-8 aerogels are shown in Figure 6c. The value of  $q_e$  increased rapidly during the initial stage of adsorption and then increased further at a relatively slow adsorption rate, before finally reaching equilibrium after approximately 260 min when the initial concentration was 100 mg/L. At an initial concentration of 40 mg/L, the aerogel reached swelling equilibrium ( $q_e$ ) after 100 min, beyond which there was almost no increase in adsorption. A higher initial concentration of the solution required a longer equilibrium swelling time. We used a pseudo-first-order and pseudo-second-order equations to analyze the mechanism of the adsorption process. These can be expressed in linear form as:

$$\ln(q_e - q_t) = \ln q_e - k_1 t, \quad (3)$$

$$\frac{t}{q_t} = \frac{1}{K_2 q_e^2} + \frac{t}{q_e} \quad (4)$$

where  $q_e$  (mg/g) is the adsorption capacity of the CNC-g-AA-2-120-8 aerogels at equilibrium,  $K_1$  ( $\text{min}^{-1}$ ) is the rate constant of the pseudo-first-order model, and  $K_2$  ( $\text{g} / \text{mg min}^{-1}$ ) is the rate constant of the pseudo-second-order model. Equations (3) and (4) were used to fit the experimental data, as shown in Figure 7a,b respectively. The kinetic parameters obtained are summarized in Table 1. For all CNC-g-AA aerogels, the calculated correlation coefficients ( $R^2$ ) were closer to unity for the pseudo second-order kinetic model than for the pseudo first-order kinetic model. Therefore, these results indicated that the dye adsorption of the CNC-g-AA-2-120-8 aerogels was described well by a pseudo-second-order kinetic model.

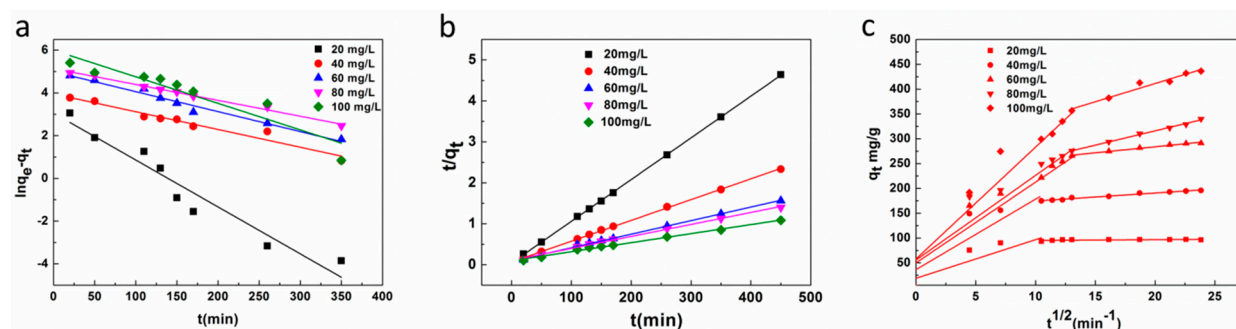


**Figure 7.** (a) Lagergren-first-order kinetic model, (b) pseudo-second-order kinetic model and (c) intra-particle diffusion model for adsorption of MB onto CNC-g-AA-2-120-8 aerogels at 25 °C.

**Table 1.** Adsorption kinetic parameters for MB adsorption of CNC-g-AA-2-120-8 aerogels.

$C_0$ (mg/L)	$q_{e,exp}$ (mg/g)	Lagergren-First-Order Kinetic Model			Pseudo-Second-Order Kinetic Mode		
		$q_{e1}$	$K_1 \times 10^{-3}$ (1/min)	$R^2$	$q_{e2}$	$K_2 \times 10^{-4}$ (g/mg min)	$R^2$
20	97.6388	96.9829	21.95	0.9240	98.1354	19.00	0.9999
40	194.8410	194.1255	8.31	0.9489	196.8505	5.50	0.9992
60	291.0470	290.5800	9.00	0.9591	302.1148	1.50	0.9972
80	383.0140	327.9173	7.43	0.9910	341.2970	1.00	0.9957
100	473.2217	416.6342	12.42	0.8629	452.4887	0.35	0.9926

We used the intra-particle diffusion model Equation (5) to further determine the mechanism of the nanocomposite gels for dye considering the diffusion of dye molecules:

$$q_t = k_i \frac{1}{2} + C \quad (5)$$

where  $K_i$  is the intra-particle diffusion rate constant ( $\text{mg/g min}^{1/2}$ ) and  $C$  is a constant related to the extent of the boundary layer effect. As shown in Figure 7c, the kinetic data also agreed well with the Elovich model, further indicating the heterogeneous chemisorption character of the CNC-g-AA-2-120-8 aerogels. Moreover, intra-particle diffusion of dye molecules played an important role at the initial stage of adsorption, as suggested by the intra-particle diffusion model fitting well with our experimental kinetic data.

### 3.5.3. Adsorption Isotherm and Thermodynamics

We determined the MB adsorption onto the CNC-g-AA-2-120-8 aerogels as a function of the equilibrium concentration of dye solution ( $C_e$ ,  $\text{mg/L}$ ). Langmuir and Freundlich isotherm equations were used to determine the isotherm parameters and linear fitting based on the two isotherm models are shown in Figure 8a,b. The obtained isotherm parameters are summarized in Table 2. The Langmuir isotherm results suggested a surplus of atoms or molecules on the adsorbent surface, the effects of MB residual valences were comparable to the molecular diameter; hence, the Langmuir isotherms describes monolayer adsorption. The Langmuir isotherm model is valid for monolayer adsorption onto a surface with a finite number of identical and equivalent sites and can be expressed in the following linear form:

$$\frac{C_e}{q_e} = \frac{1}{q_m K_L} + \frac{C_e}{q_m} \quad (6)$$

where  $q_m$  is the maximum dye adsorption onto adsorbent ( $\text{mg/g}$ ) and  $K_L$  is the Langmuir adsorption equilibrium constant ( $\text{L/g}$ ). The Freundlich isotherm model is an empirical equation that is regularly applied to multilayer adsorption, with a non-uniform distribution of adsorption heat and affinities over the heterogeneous surface of absorbent. It can be expressed in the following linear form:

$$\ln q_e = \ln K_F + \frac{1}{n} \ln C_e \quad (7)$$

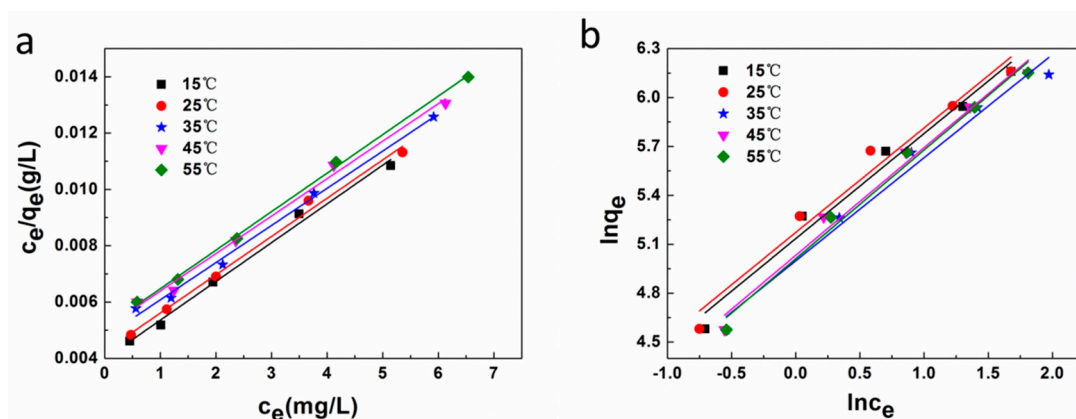


**Figure 8.** (a) Langmuir and (b) Freundlich isotherms for the adsorption of MB by CNC-g-AA-2-120-8 aerogels at different temperatures.

**Table 2.** Adsorption isotherm parameters for MB adsorption of CNC-g-AA aerogels.

T (°C)	Langmuir			Freundlich		
	$K_L$ (L/mg)	$q_{\max}$ (mg/g)	$R^2$	$K_F$	$n$	$R^2$
15	0.3467	724.6377	0.9903	169.8320	1.5524	0.9731
25	0.3200	735.2941	0.9914	176.3358	1.5596	0.9635
35	0.2773	757.5758	0.9925	148.2559	1.5818	0.9731
45	0.2628	751.8797	0.9912	153.2657	1.5139	0.9771
55	0.2681	729.9270	0.9980	150.1148	1.4996	0.9823

Three thermodynamic parameters must be considered during studies of adsorption processes, namely, enthalpy ( $\Delta H$ ), and entropy ( $\Delta S$ ). The values of  $\Delta H$  and  $\Delta S$  can be obtained by the van't Hoff equation as follows:

$$\ln K_d = \frac{\Delta S}{R} - \frac{\Delta H}{RT} \quad (8)$$

where  $R$  (8.314 J/mol K) is the universal gas constant,  $T$  (K) is the absolute temperature, and  $K_d$  is the equilibrium constant. The value of  $K_d$  can be calculated as:

$$k_d = \frac{q_e}{C_e} \quad (9)$$

The value of  $K_d$  can be determined by measurements at different temperatures, where  $q_e$  and  $C_e$  are the equilibrium concentration of the dye on the adsorbent (mg/L) and in solution (mg/L), respectively. The values of  $\Delta H$  and  $\Delta S$  can be obtained from the slope and intercept of  $\ln K_d$  versus  $1/T$ , respectively, and the free energy change  $\Delta G$  can be obtained from the following relation:

$$\Delta G = -RT \ln K_C \quad (10)$$

The  $\Delta G$ ,  $\Delta H$ , and  $\Delta S$  values of adsorption are shown in Table 3. The negative values of  $\Delta H$  confirmed that the adsorption process was exothermic in nature. The spontaneous properties and feasibility of the adsorption via physical forces as well as the high tendency of the adsorbent for the adsorbate. Thus, lower temperatures promoted adsorption of MB, which is in accordance with the results of the adsorption isotherms.

**Table 3.** Thermodynamic parameters for the adsorption of MB onto CNC-g-AA-2-120-8 aerogels.

Concentration (mg/L)	Temperature (°C)	$K_d$	$\Delta G$ (KJ/mol)	$\Delta H$ (KJ/mol)	$\Delta S$ (J/mol K)
20	15	216.7150	−12.8853	−12.4781	26.62
	25	206.7594	−13.2160		
	35	166.6885	−13.1073		
	45	166.6885	−13.5727		
	55	166.6885	−13.9580		
40	15	232.8024	−13.0569	−12.3480	22.73
	25	197.1423	−13.0979		
	35	162.6617	−13.0447		
	45	155.8044	−13.3540		
	55	146.9974	−13.6150		
60	15	149.0488	−11.8986	−11.6424	25.72
	25	144.8095	−12.3332		
	35	136.4267	−12.5940		
	45	122.1927	−12.7113		
	55	121.0599	−13.0854		
80	15	109.4590	−11.2490	−10.8564	25.72
	25	104.1624	−11.5165		
	35	97.8559	−11.7427		
	45	92.1381	−11.9645		
	55	91.1484	−12.3111		
100	15	92.2062	−10.8381	−10.5610	19.87
	25	88.3592	−11.1086		
	35	79.5277	−11.2114		
	45	76.6037	−11.4761		
	55	71.4717	−11.6477		

### 3.5.4. Adsorption and Regeneration Analysis

On the basis of the above experimental observations and our determination of the kinetic and equilibrium isotherm parameters, we propose a mechanism to describe the MB adsorption process and mechanism. Nanoscale networks with large open pores in the CNC-g-AA aerogels allowed the entry and rapid diffusion of ions and molecules, giving these materials good performance as adsorbents. The CNC-g-AA aerogel samples adsorbed MB dye through swelling and the penetration of dye into the CNC-g-AA aerogel network. The high adsorption capacity indicates strong electrostatic attractions between the dye molecules and sorbent binding sites. The surface of the CNCs and other introduced active groups also promoted electrostatic adsorption at chelating effects to remove dye molecules [51,52].

The ability to regenerate an adsorbent is an important factor for evaluating its potential practical applications. The experimental results of adsorption-desorption regeneration are shown in Figure 9. The MB removal rate and the adsorption capacity clearly decreased obviously after three adsorption-desorption experiments. After five cycles the removal ratio of MB by CNC-g-AA-2-120-8 aerogels remained greater than 83.1% and the MB adsorption capacity remained greater than 99.7 mg/g. This finding illustrates that the CNC-g-AA-2-120-8 aerogels can be reused as adsorbents for selective removal of dye pollution.

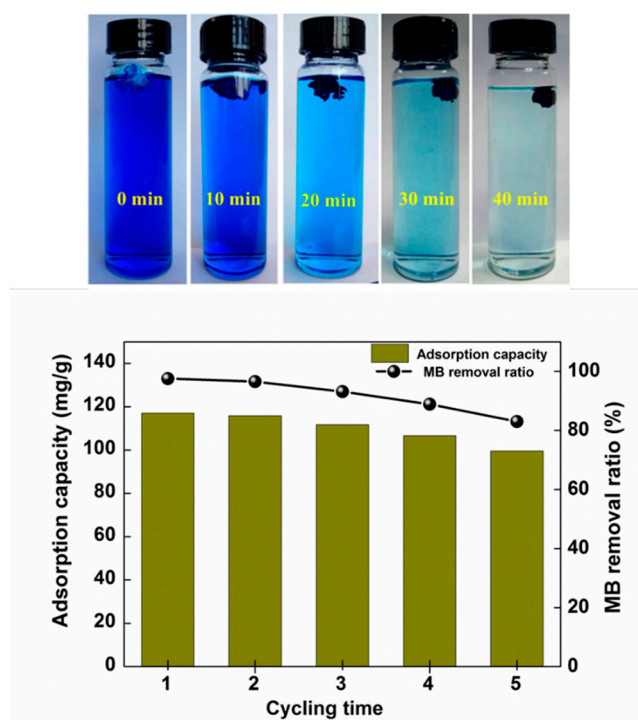


Figure 9. Adsorption and regeneration performance of CNC-g-AA-2-120-8 aerogels for MB.

## 4. Conclusions

CNC-g-AA hydro/aerogels were successfully fabricated via a hydrothermal treatment followed by freeze drying. The swelling ratio of our CNC-g-AA aerogels was as high as 495, which was much higher than other polysaccharide-g-AA aerogels systems. Adsorption isotherms indicated that the MB adsorptive behavior onto CNC-g-AA aerogels followed the Langmuir model. The kinetics of the MB adsorption followed a pseudo second-order model, suggesting that the adsorption process was chemical adsorptions dominant. The kinetic data also agreed well with the Elovich model, which further indicated the heterogeneous chemisorption character. The maximum adsorption capacity of the CNC-g-AA aerogels on MB was greater than 400 mg/g and showed excellent regeneration



ability. Our study demonstrated that the application of these CNC-g-AA aerogels can be extended to adsorption of dye contamination and agricultural residues from wastewater.

**Author Contributions:** Data curation, R.Y.; Formal analysis, M.X. and Y.Y.; Funding acquisition, S.L.; Investigation, X.L.; Methodology, C.M. and J.L.; Resources, Y.W.; Supervision, W.L. and S.L.; Validation, Q.H.; Writing—original draft, X.L. and W.L.

**Funding:** This work was financially supported by the National Natural Science Foundation of China (31500467, 31570567), the Fundamental Research Funds for the Central Universities (2572017ET02) and The First-class scientific research and innovation project of forestry engineering (201818).

**Conflicts of Interest:** There are no conflicts of interest to declare.

## References

1. Wang, W.; Bai, Q.; Liang, T.; Bai, H.; Liu, X. Two-sided surface oxidized cellulose membranes modified with PEI: Preparation, characterization and application for dyes removal. *Polymers* **2017**, *9*, 455. [[CrossRef](#)]
2. Yagub, M.T.; Sen, T.K.; Afroze, S.; Ang, H.M. Dye and its removal from aqueous solution by adsorption: A review. *Adv. Colloid Interface Sci.* **2014**, *209*, 172–184. [[CrossRef](#)] [[PubMed](#)]
3. Vijwani, H.; Nadagouda, M.N.; Namboodiri, V.; Mukhopadhyay, S.M. Hierarchical hybrid carbon nano-structures as robust and reusable adsorbents: Kinetic studies with model dye compound. *Chem. Eng. J.* **2015**, *268*, 197–207. [[CrossRef](#)]
4. Hu, E.; Shang, S.M.; Tao, X.M.; Jiang, S.X.; Chiu, K.L. Minimizing Freshwater Consumption in the Wash-Off Step in Textile Reactive Dyeing by Catalytic Ozonation with Carbon Aerogel Hosted Bimetallic Catalyst. *Polymers* **2018**, *10*, 193. [[CrossRef](#)]
5. Lee, W.J.; Clancy, A.J.; Kontturi, E.; Bismarck, A.; Shaffer, M.S. Strong and Stiff: High-Performance Cellulose Nanocrystal/Poly(vinyl alcohol) Composite Fibers. *ACS Appl. Mater. Interfaces* **2016**, *8*, 31500–31504. [[CrossRef](#)] [[PubMed](#)]
6. Klemm, D.; Kramer, F.; Moritz, S.; Lindström, T.; Ankerfors, M.; Gray, D.; Dorris, A. Nanocelluloses: A new family of nature-based materials. *Angew. Chem. Int. Ed.* **2011**, *50*, 5438–5466. [[CrossRef](#)] [[PubMed](#)]
7. Buesch, C.; Smith, S.W.; Eschbach, P.; Conley, J.F., Jr.; Simonsen, J. The Microstructure of Cellulose Nanocrystal Aerogels as Revealed by Transmission Electron Microscope Tomography. *Biomacromolecules* **2016**, *17*, 2956–2962. [[CrossRef](#)] [[PubMed](#)]
8. Yu, H.Y.; Zhang, D.Z.; Lu, F.F.; Yao, J. New Approach for Single-Step Extraction of Carboxylated Cellulose Nanocrystals for Their Use as Adsorbents and Flocculants. *ACS Sustain. Chem. Eng.* **2016**, *4*, 2632–2643. [[CrossRef](#)]
9. Liu, Q.; Jing, S.; Wang, S.; Zhuo, H.; Zhong, L.; Peng, X.; Sun, R. Flexible nanocomposites with ultrahigh specific areal capacitance and tunable properties based on a cellulose derived nanofiber-carbon sheet framework coated with polyaniline. *J. Mater. Chem. A* **2016**, *4*, 13352–13362. [[CrossRef](#)]
10. Yang, X.; Cranston, E.D. Chemically Cross-Linked Cellulose Nanocrystal Aerogels with Shape Recovery and Superabsorbent Properties. *Chem. Mater.* **2014**, *26*, 6016–6025. [[CrossRef](#)]
11. Lavoine, N.; Bergström, L. Nanocellulose-based foams and aerogels: Processing, properties, and applications. *Chem. Mater.* **2017**, *5*, 16105–16117. [[CrossRef](#)]
12. Habibi, Y.; Lucia, L.A.; Rojas, O.J. Cellulose Nanocrystals: Chemistry, Self-Assembly, and Applications. *Chem. Rev.* **2010**, *110*, 3479–3500. [[CrossRef](#)] [[PubMed](#)]
13. Miettunen, K.; Vapaavuori, J.; Tiihonen, A.; Poskela, A.; Lahtinen, P.; Halme, J.; Lund, P. Nanocellulose aerogel membranes for optimal electrolyte filling in dye solar cells. *Nano Energy* **2014**, *8*, 95–102. [[CrossRef](#)]
14. France, K.J.D.; Hoare, T.; Cranston, E.D. Review of Hydrogels and Aerogels Containing Nanocellulose. *Chem. Mater.* **2017**, *29*, 4609–4631. [[CrossRef](#)]
15. Milani, A.H.; Fielding, L.A.; Greensmith, P.; Saunders, B.R.; Adlam, D.J.; Freemont, A.J.; Hoyland, J.A.; Hodson, N.W.; Elsayy, M.A.; Miller, A.F.; et al. Anisotropic pH-Responsive Hydrogels Containing Soft or Hard Rod-Like Particles Assembled Using Low Shear. *Chem. Mater.* **2017**, *29*, 3100–3110. [[CrossRef](#)]
16. Zhang, X.; Wang, Y.; Zhao, J.; Xiao, M.; Zhang, W.; Lu, C. Mechanically Strong and Thermally Responsive Cellulose Nanofibers/Poly(N-isopropylacrylamide) Composite Aerogels. *ACS Sustain. Chem. Eng.* **2016**, *4*, 4321–4327. [[CrossRef](#)]

17. Zhao, J.; Lu, C.; He, X.; Zhang, X.; Zhang, W.; Zhang, X. Polyethylenimine-grafted cellulose nanofibril aerogels as versatile vehicles for drug delivery. *ACS Appl. Mater. Interfaces* **2015**, *7*, 2607–2615. [[CrossRef](#)] [[PubMed](#)]
18. Maleki, H. Recent advances in aerogels for environmental remediation applications: A review. *Chem. Eng. J.* **2016**, *300*, 98–118. [[CrossRef](#)]
19. Zhu, H.; Yang, X.; Cranston, E.D.; Zhu, S. Flexible and Porous Nanocellulose Aerogels with High Loadings of Metal-Organic-Framework Particles for Separations Applications. *Adv. Mater.* **2016**, *28*, 7652–7657. [[CrossRef](#)] [[PubMed](#)]
20. Javadi, A.; Zheng, Q.; Payen, F.; Javadi, A.; Altin, Y.; Cai, Z.; Sabo, R.; Gong, S. Polyvinyl alcohol-cellulose nanofibrils-graphene oxide hybrid organic aerogels. *ACS Appl. Mater. Interfaces* **2013**, *5*, 5969–5975. [[CrossRef](#)] [[PubMed](#)]
21. Maatar, W.; Boufi, S. Poly(methacrylic acid-co-maleic acid) grafted nanofibrillated cellulose as a reusable novel heavy metal ions adsorbent. *Carbohydr. Polym.* **2015**, *126*, 199–207. [[CrossRef](#)] [[PubMed](#)]
22. Dong, H.; Napadensky, E.; Orlicki, J.A.; Snyder, J.F.; Chantawansri, T.L.; Kapllani, A. Cellulose Nanofibrils and Diblock Copolymer Complex: Micelle Formation and Enhanced Dispersibility. *ACS Sustain. Chem. Eng.* **2016**, *5*, 1264–1271. [[CrossRef](#)]
23. Ma, Y.; Sun, Y.; Fu, Y.; Fang, G.; Yan, X.; Guo, Z. Swelling behaviors of porous lignin based poly (acrylic acid). *Chemosphere* **2016**, *163*, 610–619. [[CrossRef](#)] [[PubMed](#)]
24. Noppakundilokrat, S.; Choopromkaw, S.; Kiatkamjornwong, S. Hydrolyzed collagen-grafted-poly[(acrylic acid)-co-(methacrylic acid)] hydrogel for drug delivery. *Appl. Polym. Sci.* **2018**, *135*, 1–11. [[CrossRef](#)]
25. Wan, C.; Li, J. Embedding ZnO nanorods into porous cellulose aerogels via a facile one-step low-temperature hydrothermal method. *Mater. Des.* **2015**, *83*, 620–625. [[CrossRef](#)]
26. Li, W.; Wang, S.; Li, Y.; Ma, C.; Huang, Z.; Wang, C.; Li, J.; Chen, Z.; Liu, S. One-step hydrothermal synthesis of fluorescent nanocrystalline cellulose/carbon dot hydrogels. *Carbohydr. Polym.* **2017**, *175*, 7–17. [[CrossRef](#)] [[PubMed](#)]
27. Luo, R.; Chen, C.H. A one-step hydrothermal route to programmable stimuli-responsive hydrogels. *Chem. Commun.* **2015**, *51*, 6617–6620. [[CrossRef](#)] [[PubMed](#)]
28. Lewis, L.; Derakhshandeh, M.; Hatzikiriakos, S.G.; Hamad, W.Y.; MacLachlan, M.J. Hydrothermal Gelation of Aqueous Cellulose Nanocrystal Suspensions. *Biomacromolecules* **2016**, *17*, 2747–2754. [[CrossRef](#)] [[PubMed](#)]
29. Wu, X.; Shi, Z.; Fu, S.; Chen, J.; Berry, R.M.; Tam, K.C. Strategy for Synthesizing Porous Cellulose Nanocrystal Supported Metal Nanocatalysts. *ACS Sustain. Chem. Eng.* **2016**, *4*, 5929–5935. [[CrossRef](#)]
30. Dong, X.M.; Revol, J.F.; Gray, D.G. Effect of microcrystallite preparation conditions on the formation of colloid crystals of cellulose. *Cellulose* **1998**, *5*, 19–32. [[CrossRef](#)]
31. Wang, X.Y.; Zhang, Y.; Wang, S.Q.; Jiang, H.; Liu, S.; Yao, Y.; Zhang, T.M.; Li, Q. Synthesis and characterization of amine-modified spherical nanocellulose aerogels. *J. Mater. Sci.* **2018**, *53*, 13304–13315. [[CrossRef](#)]
32. Hu, K.; Sun, J.; Guo, Z.; Wang, P.; Chen, Q.; Ma, M.; Gu, N. A novel magnetic hydrogel with aligned magnetic colloidal assemblies showing controllable enhancement of magnetothermal effect in the presence of alternating magnetic field. *Adv. Mater.* **2015**, *27*, 2507–2514. [[CrossRef](#)] [[PubMed](#)]
33. Yang, L.; Jiang, X.; Ruan, W.; Zhao, B.; Xu, W.; Lombardi, J.R. Adsorption study of 4-MBA on TiO<sub>2</sub> nanoparticles by surface-enhanced Raman spectroscopy. *J. Raman Spectrosc.* **2009**, *40*, 2004–2008. [[CrossRef](#)]
34. Marrocchelli, D.; Madden, P.A.; Norberg, S.T.; Hull, S. Structural disorder in doped zirconias, part ii: Vacancy ordering effects and the conductivity maximum. *Chem. Mater.* **2011**, *23*, 1365–1373. [[CrossRef](#)]
35. Chau, M.; De France, K.J.; Kopera, B.; Machado, V.R.; Rosenfeldt, S.; Reyes, L.; Chan, K.J.W.; Förster, S.; Cranston, E.D.; Hoare, T.; et al. Composite Hydrogels with Tunable Anisotropic Morphologies and Mechanical Properties. *Chem. Mater.* **2016**, *28*, 3406–3415. [[CrossRef](#)]
36. Jayakumar, R.; Prabakaran, M.; Reis, R.L.; Mano, J.F. Graft copolymerized chitosan-present status and applications. *Carbohydr. Polym.* **2005**, *62*, 142–158. [[CrossRef](#)]
37. Kumar, A.; Rao, K.M.; Han, S.S. Synthesis of mechanically stiff and bioactive hybrid hydrogels for bone tissue engineering applications. *Chem. Eng. J.* **2017**, *317*, 119–131. [[CrossRef](#)]
38. Fu, J.; Wang, S.; He, C.; Lu, Z.; Huang, J.; Chen, Z. Facilitated fabrication of high strength silica aerogels using cellulose nanofibrils as scaffold. *Carbohydr. Polym.* **2016**, *147*, 89–96. [[CrossRef](#)] [[PubMed](#)]

39. Yang, J.; Han, C.R.; Zhang, X.M.; Xu, F.; Sun, R.C. Cellulose Nanocrystals Mechanical Reinforcement in Composite Hydrogels with Multiple Cross-Links: Correlations between Dissipation Properties and Deformation Mechanisms. *Macromolecules* **2014**, *47*, 4077–4086. [[CrossRef](#)]
40. Tang, L.R.; Huang, B.; Yang, N.T.; Li, T.; Lu, Q.L.; Lin, W.Y.; Che, X.R. Organicsolvent-free and efficient manufacture of functionalized cellulose nanocrystals via one-pot tandem reactions. *Green. Chem.* **2013**, *15*, 2369–2373. [[CrossRef](#)]
41. Das, D.; Ghosh, P.; Dhara, S.; Panda, A.B.; Pal, S. Dextrin and Poly(acrylic acid)-Based Biodegradable, Non-Cytotoxic, Chemically Cross-Linked Hydrogel for Sustained Release of Ornidazole and Ciprofloxacin. *ACS Appl. Mater. Interfaces* **2015**, *7*, 4791–4803. [[CrossRef](#)] [[PubMed](#)]
42. Spagnol, C.; Rodrigues, F.H.A.; Pereira, A.G.B.; Fajardo, A.R.; Rubira, A.F.; Muniz, E.C. Superabsorbent hydrogel nanocomposites based on starch-g-poly(sodium acrylate) matrix filled with cellulose nanowhiskers. *Cellulose* **2012**, *19*, 1225–1237. [[CrossRef](#)]
43. Chau, M.; Sriskandha, S.E.; Pichugin, D.; Therien-Aubin, H.; Nykypanchuk, D.; Chauve, G.; Methot, M.; Bouchard, J.; Gang, O.; Kumacheva, E. Ion-Mediated Gelation of Aqueous Suspensions of Cellulose Nanocrystals. *Biomacromolecules* **2015**, *16*, 2455–2462. [[CrossRef](#)] [[PubMed](#)]
44. Fatona, A.; Berry, R.M.; Brook, M.A.; Moran-Mirabal, J.M. Versatile Surface Modification of Cellulose Fibers and Cellulose Nanocrystals through Modular Triazinyl Chemistry. *Chem. Mater.* **2018**, *30*, 2424–2435. [[CrossRef](#)]
45. Mukerabigwi, J.F.; Lei, S.; Fan, L.; Wang, H.; Luo, S.; Ma, X.; Qin, J.; Huang, X.; Cao, Y. Eco-friendly nano-hybrid superabsorbent composite from hydroxyethyl cellulose and diatomite. *RSC Adv.* **2016**, *6*, 31607–31618. [[CrossRef](#)]
46. Yang, J.; Han, C.R.; Duan, J.F.; Ma, M.G.; Zhang, X.M.; Xu, F.; Sun, R.C.; Xie, X.M. Studies on the properties and formation mechanism of flexible nanocomposite hydrogels from cellulose nanocrystals and poly(acrylic acid). *J. Mater. Chem.* **2012**, *22*, 22467–22480. [[CrossRef](#)]
47. Chen, W.; Li, Q.; Wang, Y.; Yi, X.; Zeng, J.; Yu, H.; Liu, Y.; Li, J. Comparative study of aerogels obtained from differently prepared nanocellulose fibers. *ChemSusChem* **2014**, *7*, 154–161. [[CrossRef](#)] [[PubMed](#)]
48. Fumagalli, M.; Ouhab, D.; Boisseau, S.M.; Heux, L. Versatile gas-phase reactions for surface to bulk esterification of cellulose microfibrils aerogels. *Biomacromolecules* **2013**, *14*, 3246–3255. [[CrossRef](#)] [[PubMed](#)]
49. Zeng, M.; Echols, I.; Wang, P.; Lei, S.; Luo, J.; Peng, B.; He, L.; Zhang, L.; Huang, D.; Mejia, C.; et al. Highly Biocompatible, Underwater Superhydrophilic and Multifunctional Biopolymer Membrane for Efficient Oil-Water Separation and Aqueous Pollutant Removal. *ACS Sustain. Chem. Eng.* **2018**, *6*, 3879–3887. [[CrossRef](#)]
50. Štefelová, J.; Slovák, V.; Siqueira, G.; Olsson, R.T.; Tingaut, P.; Zimmermann, T.; Sehaqui, H. Drying and Pyrolysis of Cellulose Nanofibers from Wood, Bacteria, and Algae for Char Application in Oil Absorption and Dye Adsorption. *ACS Sustain. Chem. Eng.* **2017**, *5*, 2679–2692. [[CrossRef](#)]
51. He, X.; Male, K.B.; Nesterenko, P.N.; Brabazon, D.; Paull, B.; Luong, J.H. Adsorption and desorption of methylene blue on porous carbon monoliths and nanocrystalline cellulose. *ACS Appl. Mater. Interfaces* **2013**, *5*, 8796–8804. [[CrossRef](#)] [[PubMed](#)]
52. Yang, H.; Sheikhi, A.; van de Ven, T.G. Reusable Green Aerogels from Cross-Linked Hairy Nanocrystalline Cellulose and Modified Chitosan for Dye Removal. *Langmuir* **2016**, *32*, 11771–11779. [[CrossRef](#)] [[PubMed](#)]

